Cell Reports
Medicine

Article

Metformin pretreatment rescues olfactory memory associated with subependymal zone neurogenesis in a juvenile model of cranial irradiation

Graphical abstract

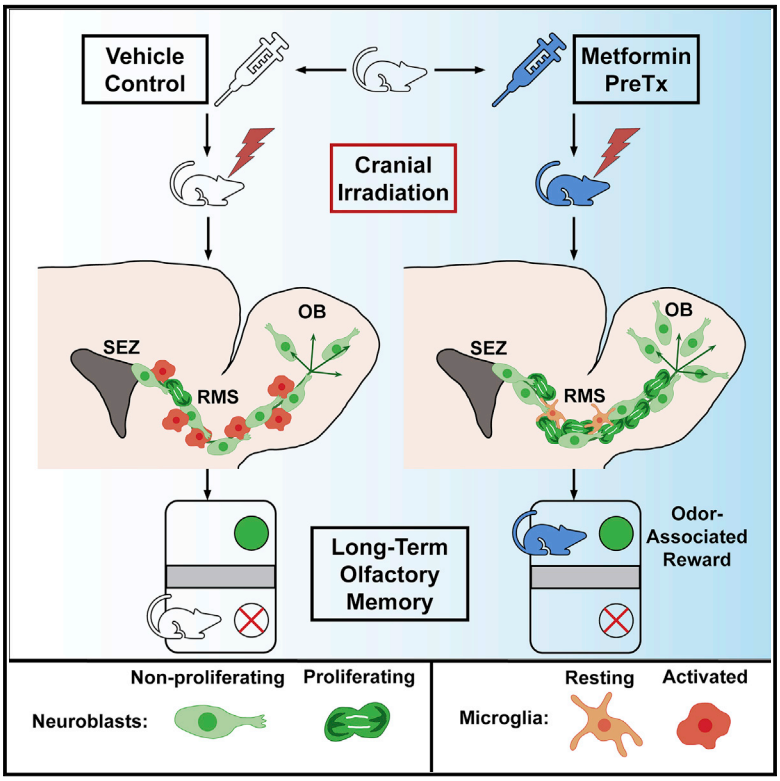

Highlights

- Cranial IR in juvenile mice impairs subependymal zone-olfactory bulb neurogenesis
- IR-induced deficits are associated with long-term olfactory memory impairments
- Metformin pretreatment (preTx) rescues neurogenesis and long-term olfactory memory
- Metformin preTx attenuates the inflammatory response in the neurogenic niche

Authors

Daniel Derkach, Tarlan Kehtari, Matthew Renaud, Mohsen Heidari, Nishanth Lakshman, Cindi M. Morshead

Correspondence

cindi.morshead@utoronto.ca

In brief

Derkach et al. show that metformin administration prior to cranial irradiation (IR) in juvenile mice protects against radiation-induced neurogenic deficits, inflammation, and impairments in olfactory memory. Metformin pretreatment is a potential prophylactic intervention to protect against radiation-induced deficits.

Derkach et al., 2021, Cell Reports Medicine 2, 100231
April 20, 2021
https://doi.org/10.1016/j.xcrm.2021.100231

CellPress

Cell Reports Medicine

CellPress
OPEN ACCESS

Article

Metformin pretreatment rescues olfactory memory associated with subependymal zone neurogenesis in a juvenile model of cranial irradiation

Daniel Derkach,[1,2] Tarlan Kehtari,[2,5] Matthew Renaud,[2,5] Mohsen Heidari,[2] Nishanth Lakshman,[1,2] and Cindi M. Morshead[1,2,3,4,6,*]

[1]Institute of Medical Science, University of Toronto, Toronto, ON, Canada
[2]Terrence Donnelly Centre for Cellular and Biomolecular Research, University of Toronto, Toronto, ON, Canada
[3]Division of Anatomy, Department of Surgery, University of Toronto, Toronto, ON, Canada
[4]Institute of Biomedical Engineering, University of Toronto, Toronto, ON, Canada
[5]These authors contributed equally
[6]Lead contact
*Correspondence: cindi.morshead@utoronto.ca
https://doi.org/10.1016/j.xcrm.2021.100231

SUMMARY

Cranial irradiation (IR) is an effective adjuvant therapy in the treatment of childhood brain tumors but results in long-lasting cognitive deficits associated with impaired neurogenesis, as evidenced in rodent models. Metformin has been shown to expand the endogenous neural stem cell (NSC) pool and promote neurogenesis under physiological conditions and in response to neonatal brain injury, suggesting a potential role in neurorepair. Here, we assess whether metformin pretreatment, a clinically feasible treatment for children receiving cranial IR, promotes neurorepair in a mouse cranial IR model. Using immunofluorescence and the *in vitro* neurosphere assay, we show that NSCs are depleted by cranial IR but spontaneously recover, although deficits to proliferative neuroblasts persist. Metformin pretreatment enhances the recovery of neurogenesis, attenuates the microglial response, and promotes recovery of long-term olfactory memory. These findings indicate that metformin is a promising candidate for further preclinical and clinical investigations of neurorepair in childhood brain injuries.

INTRODUCTION

Cranial irradiation (IR) is commonly used as an adjuvant therapy in the treatment of childhood primary brain tumors. Although the use of cranial IR has led to improved patient survival rates, it is associated with late cognitive impairments affecting attention, memory, and academic performance.[1–4] Furthermore, cranial IR-associated cognitive impairments typically worsen over several years and arise more rapidly in children who receive cranial IR at younger ages.[5,6] There are presently no effective prophylactic measures or treatments available for mitigating these cognitive impairments following childhood IR.

Studies using preclinical animal models have suggested that the cause of cranial-IR-induced cognitive impairments is associated with neural stem cell (NSC) dysfunction and deficits to neurogenesis.[7,8] In the postnatal mammalian brain, NSCs predominantly reside in the subependymal zone (SEZ) adjacent to the ependymal cell layer lining the lateral ventricles (also known as the subventricular zone), as well as in the subgranular zone of the hippocampal dentate gyrus, where they contribute to neurogenesis throughout life.[9,10] Although hippocampal neurogenesis has been implicated in various forms of learning, memory, and affective behaviors that are relevant to cranial-IR-associated cognitive impairments, several discrepancies persist among correlative and ablation studies, making it critical to assess the function of hippocampal neurogenesis using a battery of cognitive tests.[10] Under normal physiological conditions, SEZ NSCs give rise to progeny that generate neuroblasts, which migrate along the rostral migratory stream (RMS) to the olfactory bulb (OB),[11,12] where they mature to become inhibitory GABAergic interneurons that underlie olfactory memory.[13,14] Importantly, NSCs and their progeny (together termed neural precursor cells) interact with their niche to effectively regulate their behavior under homeostatic conditions, in aging, and in response to injury.[15–18]

The significant roles of endogenous NSCs and neurogenesis in the postnatal brain underlie the importance of ensuring they are maintained throughout life. Notably, neural precursor cells are particularly vulnerable to IR-induced DNA double-stranded breaks and apoptosis due to their proliferative activity *in vivo*.[19,20] Cell death occurs within hours following IR doses as low as 2 Gy,[21,22] and surviving NSCs undergo cellular senescence reminiscent of NSCs in the aging SEZ that have reduced proliferative and neurogenic capacity.[23–25] Cranial IR also perturbs the neurogenic niche, resulting in acute and sustained microglial activation, increased oxidative stress, and disrupted microvascular

angiogenesis.[7,26,27] Neuroinflammation alone is sufficient to reduce neurogenesis and may play a significant role in the response to cranial IR.[28,29] Indeed, changes to the neurogenic niche may be paramount in determining the rate or extent of recovery, as studies have shown that hippocampal neurogenesis does not recover following cranial IR, although SEZ NSCs repopulate over time despite persistent deficits to OB neurogenesis.[30,31] Finally, numerous studies have demonstrated that cranial-IR-induced depletion of NSCs and their proliferating progeny is associated with cognitive impairments, including deficits to long-term olfactory memory.[8,32] Together, these results suggest that therapeutic interventions should aim to promote neurogenesis in an irradiated neurogenic niche, mitigate or repair damage to the niche, or both.

To promote brain repair and functional recovery, activation of endogenous neural precursor cells has demonstrated some success.[33] The antidiabetic drug metformin has recently been shown to increase the size of the NSC pool and promote neurogenesis in mice, resulting in improved spatial memory formation under homeostasis,[34] as well as promoting cognitive and motor functional recovery following neonatal stroke.[35,36] Further, as an activator of AMP-activated protein kinase,[37,38] metformin has pleiotropic effects in the central nervous system, acting on various cell types, leading to increased angiogenesis, anti-inflammatory microglia activity,[39–41] as well as the inhibition of nuclear factor kappa B (NF-κB)-mediated inflammation and mTOR signaling.[42–44]

Herein, we investigated the effects of metformin pretreatment (preTx) in a model of juvenile cranial IR[8] that involves a clinically relevant dose of IR (8 Gy)[45] and age (postnatal day 17 [P17]).[5,46] Using an *in vitro* NSC colony-forming assay (neurosphere assay), we assessed the effects of metformin preTx and cranial IR on the activated NSC (aNSC) pool (i.e., colony-forming NSCs *in vitro*)[47] and quantified neurogenesis and microglia activation along the SEZ-OB neurogenic axis *in vivo*. Additionally, we assessed behavioral outcomes following cranial IR and metformin preTx using a long-term olfactory memory task. We identified acute deficits in the size of the SEZ NSC pool, which were partly attributed to a disrupted neurogenic niche. Although the size of the NSC pool recovered spontaneously over time, deficits to neuroblast proliferation persisted following cranial IR. Notably, metformin preTx enhanced neuroblast proliferation over this same time period, leading to a rescue of newborn neurons in the OB. Most strikingly, metformin preTx led to a complete recovery of long-term olfactory memory post-cranial IR. Overall, the cellular and behavioral recovery were associated with decreased microglial activation along the RMS. Together, these findings demonstrate that metformin preTx is a promising strategy to minimize neural impairments that result from juvenile cranial IR.

RESULTS

Metformin transiently expands the neonatal, but not the juvenile, SEZ NSC pool

With the goal of administering metformin to enhance recovery in a model of juvenile cranial IR, we first sought to determine an optimal administration window for metformin in the prepubescent mouse. Because neurogenesis and functional recovery following neonatal brain injury has been correlated with an expansion of the NSC pool,[35,36] we hypothesized that expanding the endogenous NSC pool would provide an effective means by which to protect and/or rescue neurogenesis following cranial IR. We administered metformin via subcutaneous injection once daily (200 mg/kg/day) for 7 days in both male and female mice, beginning on P9 or P18, ages that reflect a potential preTx (P9) and post-treatment (P18) start date in a model of juvenile cranial IR.[8] The neurosphere assay was performed 1 day after the final metformin injection, and the number of clonally derived neurospheres was quantified (Figure 1A). Similar to previous findings, 7 days of metformin administration starting on P9 significantly increased the number of SEZ-derived neurospheres formed relative to phosphate-buffered saline (PBS)-treated controls in both male (∼49% increase [Ctrl = 47.41 ± 2.99; Met = 71.44 ± 9.36 neurospheres]) and female (∼42% increase [Ctrl = 54.54 ± 5.95; Met = 78.29 ± 8.23 neurospheres]) mice (Figure 1B). Administration of metformin for 7 days starting on P18 did not significantly expand the size of the NSC pool (Ctrl = 42.06 ± 2.84; Met = 50.83 ± 6.09 neurospheres; Figure 1C).[36]

We next asked whether the NSC pool expansion was transient or persisted after metformin administration was complete. The neurosphere assay was performed on P16, P19, P25, or P47 following P9–P15 metformin treatment (Figure 1D). The metformin-induced increase in neurosphere formation was significantly elevated (∼28% increase) until P19 and returned to baseline by P47 (Figure 1E). Based on the observation that metformin treatment from P9 to P15 promoted an increase in neurosphere formation, and that this expansion persisted beyond the date of cranial IR (P17), this preTx paradigm was used for subsequent experiments.

Metformin pretreatment does not affect the acute depletion or recovery of SEZ NSCs following juvenile cranial IR

Metformin preTx has been shown to confer neuroprotection against both stroke and spinal cord injury.[43,44,48] Most importantly, administration prior to cranial IR is a feasible approach in a clinical setting. Hence, we examined the efficacy of a metformin preTx paradigm whereby mice receive metformin from P9 to P15 and juvenile cranial IR on P17. First, to characterize the acute and chronic effects of juvenile cranial IR on the SEZ NSC pool, mice were sacrificed for the neurosphere assay 2, 8, or 30 days post-IR and compared with age-matched non-irradiated controls (P19, P25, and P47, respectively; Figure 2A). A significant reduction in SEZ-derived neurosphere formation was observed 2 days post-IR relative to non-irradiated controls (∼51% reduction), and the number of neurospheres partially recovered at 8 days post-IR (∼21% reduction). By 30 days post-IR, there was no significant difference in neurosphere formation between irradiated and non-irradiated mice, indicating that the NSC pool spontaneously recovered over time (Figure 2B). Interestingly, metformin preTx did not prevent the acute deficit to neurosphere formation 2 days post-IR or enhance neurosphere formation at 8 or 30 days post-IR relative to untreated mice (Figure 2B).

We also examined neurosphere formation following metformin preTx extending until 1 day post-IR (Figure S1A) or following

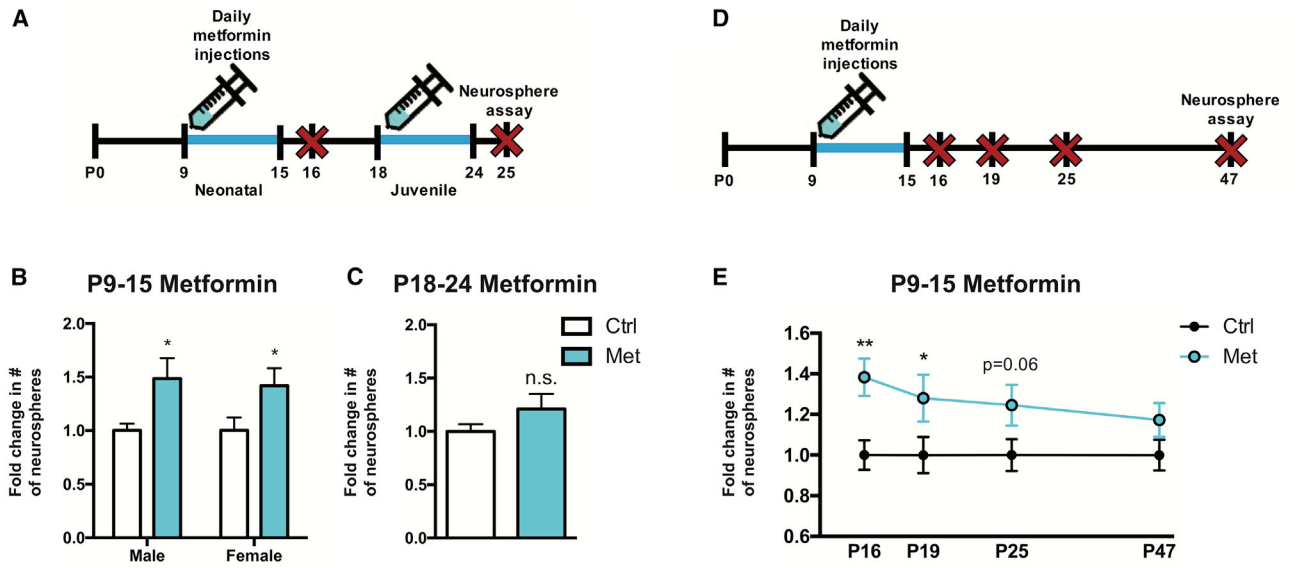

Figure 1. Metformin transiently expands the neonatal, but not the juvenile, SEZ NSC pool

(A) Experimental timeline for assessing SEZ NSC pool size following 7-day metformin administration in neonatal (P9–P15) or juvenile (P18–P24) mice.

(B and C) Fold change in the number of SEZ-derived neurospheres 1 day after (B) P9–P15 metformin administration (n = 7–9 mice/group; *p < 0.05; unpaired t test) and (C) P18–P24 metformin administration (n = 8–9 mice/group; p = 0.195; unpaired t test).

(D) Experimental timeline for assessing the longitudinal effects of P9–P15 metformin administration on SEZ NSC pool size.

(E) Fold change in the number of SEZ-derived neurospheres at various endpoints following P9–P15 metformin administration (n = 7–17 mice/group; P16: **p < 0.01; P19: *p < 0.05; P25: p = 0.062; P47: p = 0.293; unpaired t test).

Data are presented as mean ± SEM.

7 days of metformin treatment starting 1 day post-IR (Figure S1C). Neither treatment paradigm rescued the IR-induced deficits to neurosphere formation (Figures S1B and S1D). Hence, metformin treatment is insufficient to rescue the loss or accelerate the spontaneous recovery of the SEZ NSC pool following cranial IR.

To assess the effect of metformin preTx on the activation state of NSCs following cranial IR, GFAP::GFP mice[49] were sacrificed 2 days post-IR to quantify the ratio of GFAP::GFP$^+$CD133$^+$EGFR$^-$ quiescent NSCs (qNSCs) and GFAP::GFP$^+$CD133$^+$EGFR$^+$ activated NSCs (aNSCs) via fluorescence-activated cell sorting (FACS) (Figures S2A–S2C).[47] Approximately 60% of NSCs were activated in control mice, and no significant differences were observed in cranial IR mice, regardless of metformin preTx (Figure S2D).

Metformin pretreatment enhances the recovery of neuroblast proliferation in the SEZ and RMS

We next asked whether metformin preTx could prevent the deficits and/or enhance the recovery of proliferating neuroblasts post-IR. Proliferating neuroblasts in the SEZ were quantified 2 and 30 days post-IR using the neuroblast marker doublecortin (DCX) and the proliferation marker Ki67 (Figures 3A and 3B). We observed a complete loss of DCX$^+$Ki67$^+$ neuroblasts in the SEZ at 2 days post-IR and a near-complete loss in metformin preTx mice (Figures 3B and 3C). DCX$^+$Ki67$^+$ cells were observed in both treated and untreated mice by 30 days post-IR; however, although a significant ~33% reduction persisted in untreated mice, metformin preTx completely rescued this deficit (Figure 3D). A similar rescue of DCX$^+$Ki67$^+$ cells was observed along the RMS at 30 days post-IR in metformin preTx mice (Figures 3E and 3F). Interestingly, metformin preTx did not significantly alter the total number of neuroblasts (DCX$^+$) or proliferating (Ki67$^+$) cells in the SEZ (Figure S3), suggesting that metformin preTx specifically supported the recovery of proliferating neuroblasts following cranial IR.

Metformin pretreatment enhances OB neurogenesis and rescues long-term olfactory memory

To ask whether the recovery of proliferating neuroblasts resulted in OB neurogenesis and was associated with functional recovery, we performed a long-term olfactory memory (LTOM) task. We used a sand-digging-based olfactory discrimination/learning assay to assess both the acquisition of an odor-reward association and retention (memory) of this association and quantified newborn neuroblasts and neurons in the OB at the end of the LTOM assessment (Figures 4A and 4B). Briefly, to assess these behaviors, mice were trained for 8 days (8 trials/day) to associate an odorant with a sugar reward at 30 days post-IR (P47–P54).[14,50] Mice from each group that correctly chose the reward-associated odorant at an average rate of >80% over the final 2 acquisition days were subsequently tested in the LTOM task 30 days following acquisition (P84). This cutoff was to ensure that only mice that acquired the task would later be tested for retention. As shown in Figure 4C, mice that received cranial IR alone displayed a deficit on the 6th day of training, suggesting a delay in the acquisition of the task, but importantly, no significant differences were observed in the final 2 acquisition

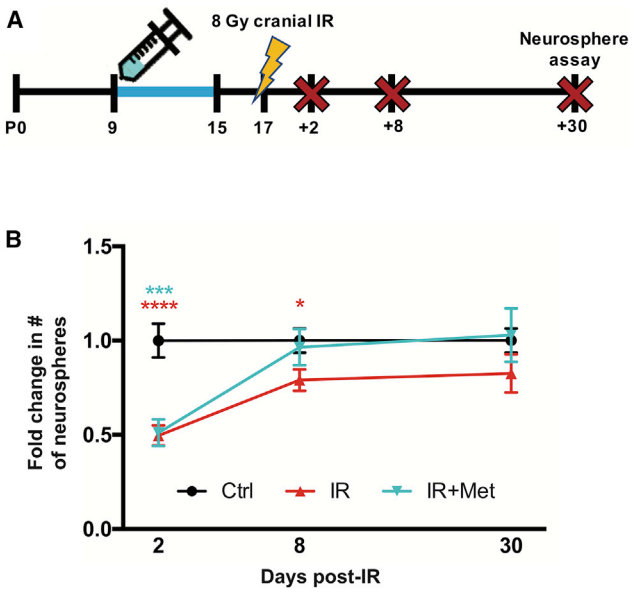

Figure 2. Metformin preTx does not affect the acute depletion or recovery of SEZ NSCs following juvenile cranial IR

(A) Experimental timeline for assessing the effects of metformin preTx and P17 cranial IR on SEZ NSC pool size.

(B) Fold change in the number of SEZ-derived neurospheres following metformin preTx and P17 cranial IR (2 days post-IR: n = 11–18 mice/group [Ctrl versus IR ****$p < 0.0001$; Ctrl versus IR+Met ***$p < 0.001$; one-way ANOVA with Tukey's test]; 8 days post-IR: n = 13–18 mice/group [Ctrl versus IR *$p < 0.05$, unpaired t test]; 30 days post-IR: n = 7–10 mice/group).

Data are presented as mean ± SEM.

See also Figures S1 and S2.

days between any of the groups. Despite the ability to acquire the task, mice that received juvenile cranial IR alone did not perform significantly greater than chance (50%) levels upon LTOM testing at P84. Most strikingly, this deficit was completely rescued by metformin preTx (Figure 4D).

We examined neurogenesis in these same cohorts. Mice received daily injections of 5-ethynyl-2′-deoxyuridine (EdU) at the end of the acquisition phase (P54–P57), and the number of label-retaining EdU^+DCX^+ neuroblasts and EdU^+NeuN^+ newborn neurons were subsequently quantified following LTOM assessment on P84. Interestingly, mice that received metformin preTx displayed a ~96% increase in EdU^+DCX^+ neuroblasts relative to untreated irradiated mice (Figures 4E and 4F). Furthermore, we observed a significant 33% reduction ($p = 0.021$) in EdU^+NeuN^+ newborn neurons following cranial IR, although there was no significant reduction ($p = 0.396$) in mice that received metformin preTx (Figure 4G). Together, these data reveal that metformin preTx rescues SEZ-OB neurogenesis and LTOM following juvenile cranial IR.

Cranial IR and metformin-induced changes in the microenvironment are sufficient to regulate neural precursor cell behavior

We next asked whether factors from the juvenile irradiated SEZ niche were sufficient to reduce neurosphere formation and whether metformin preTx was able to alter the potential environmental impact on neurosphere formation at early times post-IR. To address this question, neurospheres derived from the SEZ of non-irradiated juvenile mice were grown in conditioned media that was generated from the SEZ of non-irradiated or cranially irradiated mice with or without preTx (Figure 5A). We found that conditioned media derived from SEZ cultures of cranially irradiated mice significantly reduced neurosphere formation (Figure 5B), suggesting that irradiation-induced changes in the niche are sufficient for regulating NSC behavior. Consistent with the finding that metformin preTx did not rescue neurosphere depletion following cranial IR (Figure 2), conditioned media from metformin-pretreated irradiated mice did not rescue neurosphere numbers.

Although the depletion and recovery of neurospheres were not altered by metformin preTx, we observed an effect on the neural stem cell progeny at later times, most notably along the RMS (Figure 3F). Cranial IR has been reported to induce neuroinflammation associated with reduced hippocampal neurogenesis;[7,29,51] hence, we predicted that cranial IR-induced deficits along the RMS would be associated with increased inflammation. We quantified the number of $Iba1^+CD68^+$ activated microglia and $Iba1^+Ki67^+$ proliferating microglia along the RMS at 30 days post-IR (Figure 5C), where we saw the greatest deficit to neuroblast proliferation (Figure 3F). Cranial IR induced a significant increase in activated (~10-fold) and proliferating (~13-fold) microglia compared to non-irradiated controls, and most interestingly, this increase was absent in mice that received metformin preTx (Figures 5D–5F). Hence, metformin preTx significantly attenuates the inflammatory response along the RMS, which is associated with enhanced SEZ-OB neurogenesis and long-term olfactory memory following juvenile cranial IR.

DISCUSSION

The findings presented in this study advance our understanding of IR-induced changes in neurogenesis and behavioral deficits in rodents.[7,30,32,52] Most importantly, our findings support a prophylactic role for metformin in attenuating neurogenic deficits and promoting functional recovery following juvenile cranial IR in a clinically relevant rodent model. Although the SEZ NSC pool recovered spontaneously following juvenile cranial IR, the proliferative behavior of NSC progeny was impaired along the SEZ-OB neurogenic axis. Importantly, metformin preTx was sufficient to rescue these deficits to neuroblast proliferation, enhance neuroblast arrival in the OB, and completely rescue LTOM. In addition, we demonstrated that secreted factors in the irradiated SEZ niche are sufficient to induce deficits to the NSC pool *in vitro* and that IR-induced deficits to neuroblast proliferation in the RMS are strongly associated with increased microglial proliferation, which is also attenuated with metformin preTx. These findings highlight metformin's pleiotropic effects and demonstrate the importance of understanding how stem cell niches regulate stem cell behavior.

Our observation that neonatal, but not juvenile, metformin administration caused an expansion of the SEZ NSC pool confirms recent findings of age-dependent effects on NSCs and their neurogenic niche, whereby metformin administration for

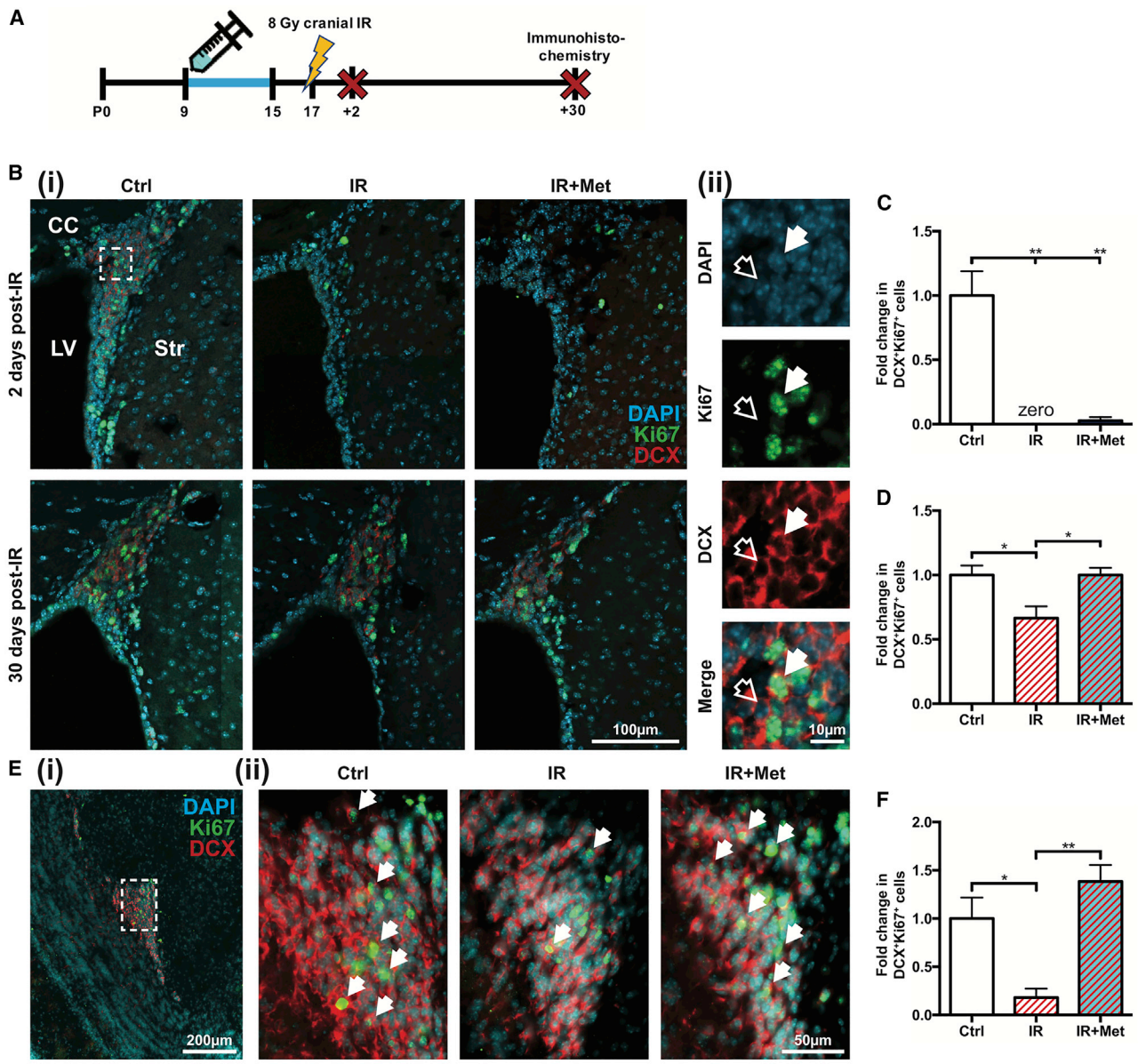

Figure 3. Metformin preTx enhances the recovery of neuroblast proliferation in the SEZ and RMS

(A) Experimental timeline for assessing the effects of metformin preTx and cranial IR on DCX$^+$Ki67$^+$ neuroblasts.

(B) (i) Representative tiled images of the dorsolateral corner of the SEZ at 2 and 30 days post-IR (scale bar represents 100 μm; blue, DAPI; green, Ki67; red, DCX). (ii) High-power images of white box in (i) (solid arrow, DCX$^+$Ki67$^+$ cell; empty arrow, DCX$^+$Ki67$^-$ cell; scale bar represents 10 μm).

(C and D) Fold change in the number of DCX$^+$Ki67$^+$ neuroblasts in the SEZ following metformin preTx and cranial IR at (C) 2 days post-IR and (D) 30 days post-IR (n = 3–4 mice/group).

(E) Representative images of the RMS at 30 days post-IR (arrows, examples of DCX$^+$Ki67$^+$ cell; i, scale bar represents 200 μm; ii, scale bar represents 50 μm).

(F) Fold change in the number of DCX$^+$Ki67$^+$ neuroblasts in the RMS at 30 days post-IR (n = 3 mice/group). *p < 0.05; **p < 0.01; one-way ANOVA with Tukey's test. Data are presented as mean ± SEM. CC, corpus callosum; LV, lateral ventricle; Str, striatum.

See also Figure S3.

up to 25 days did not expand the SEZ NSC pool in juvenile mice.[31,36] Interestingly, we observed that expansion of the pool is transient *in vivo*, which was not predicted based on previous studies revealing continued expansion of passaged neurospheres in the absence of metformin derived from primary neurospheres initially exposed to metformin.[53] The differences observed in the expansion of the NSC pool likely highlight the different effects of *in vivo* versus *in vitro* metformin exposure on NSCs. Indeed, it has recently been shown that NSCs in the juvenile SEZ undergo high levels of consuming symmetric divisions, giving rise to progeny that generate OB neurons at the expense of the NSC pool.[54] Hence, it is possible that, during

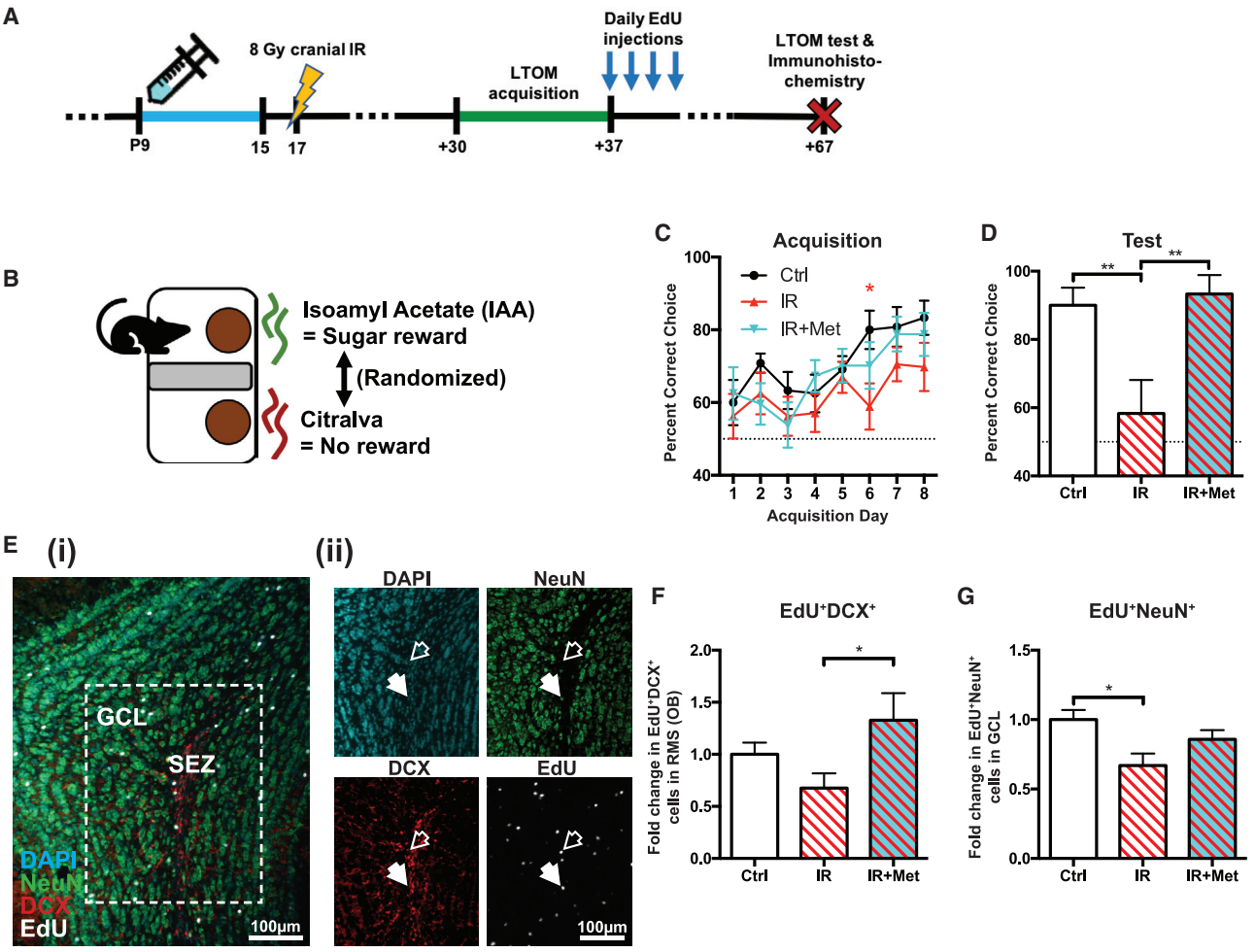

Figure 4. Metformin preTx enhances OB neurogenesis and rescues LTOM

(A) Experimental timeline for assessing the effects of metformin preTx and cranial IR on LTOM and the arrival of neuroblasts in the OB that were generated at the end of LTOM acquisition/training.

(B) Schematic of LTOM task setup.

(C and D) Percentage of trials in which mice correctly chose the isoamyl acetate (IAA)-scented dish containing the odor-paired reward during (C) LTOM acquisition (n = 15 Ctrl, 14 IR, and 13 IR+Met mice; *p < 0.05 Ctrl versus IR, repeated-measures ANOVA with Tukey's test) and (D) LTOM testing (n = 10 Ctrl, 6 IR, and 9 IR+Met mice; **p < 0.01, one-way ANOVA with Tukey's test; dotted line = chance [50%]). Only mice that scored >80% over the final 2 acquisition days (C) were tested (D).

(E) Representative images of the OB (scale bar represents 100 μm; blue, DAPI; green, NeuN; red, DCX; white, EdU). (ii) Single channel images of white box in (i) (solid arrow, EdU^+NeuN^+ cell; empty arrow, EdU^+DCX^+ cell).

(F and G) Fold change in the number of (F) EdU^+DCX^+ neuroblasts in the OB core (RMS) and (G) EdU^+NeuN^+ newborn neurons in the OB granule cell layer (GCL) 30 days after the end of LTOM acquisition (n = 5 mice/group; *p < 0.05; one-way ANOVA with Tukey's test).

Data are presented as mean ± SEM.

juvenile development, the neurogenic niche is more conducive to NSC lineage progression than self-renewal, resulting in the transience of metformin's expansion of the neonatal NSC pool.

Expansion of the NSC pool in response to metformin treatment has been reported to be due to TAp73-dependent proliferation, as well as attributed to enhanced cell survival.[53] Alternatively, metformin administration may increase neurosphere formation by stimulating the conversion of qNSCs to aNSCs.[47] Interestingly, our findings demonstrate that the ratio of qNSCs and aNSCs at P19 is not altered by P17 cranial IR (with or without metformin preTx). This finding supports the hypothesis that both the qNSC and aNSC pools are diminished to similar extents following IR. Previous reports show that NSCs self-regulate their activation through negative feedback,[55,56] and numerous studies report niche-mediated effects on NSC quiescence and activation,[57–61] thereby implicating multiple mechanisms that may contribute to, or compete with, metformin's effects on NSC behavior.

Our observation that SEZ-derived neurosphere formation spontaneously recovered 30 days post-IR is in agreement with previous studies that used putative SEZ NSC markers *in vivo* and similarly show the spontaneous recovery of the NSC pool.

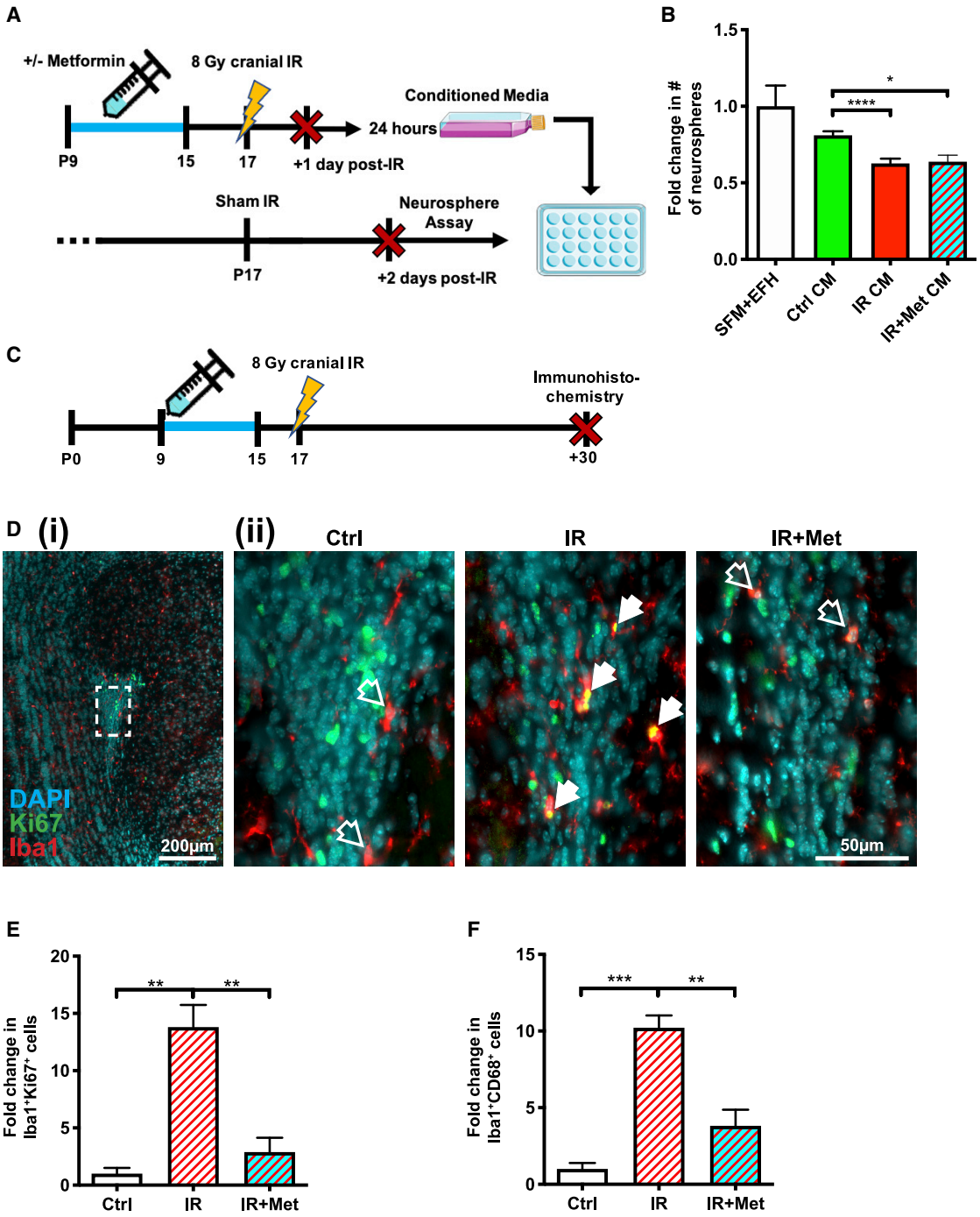

Figure 5. Juvenile cranial IR induces the secretion of factors that reduce SEZ-derived neurosphere formation and increases microglial proliferation in the RMS

(A) Experimental timeline for assessing the effects of conditioned media from the irradiated SEZ, with and without metformin pretreatment, on neurospheres derived from the non-irradiated SEZ.

(B) Fold change in the number of SEZ-derived neurospheres grown in normal growth media (serum-free media [SFM] + epidermal growth factor + basic fibroblast growth factor + heparin [EFH]), conditioned media (CM) from non-irradiated controls (Ctrl), CM from cranially irradiated mice (IR), and CM from cranially irradiated mice that received metformin pretreatment (IR+Met) (n = 4–9 mice/group; *$p < 0.05$; ****$p < 0.0001$; one-way ANOVA with Tukey's test).

(C) Experimental timeline for assessing the effects of metformin preTx and cranial IR on proliferating Iba1$^+$Ki67$^+$ and activated Iba1$^+$CD68$^+$ microglia in the RMS.

(legend continued on next page)

Notably, spontaneous NSC recovery is not correlated with the proliferation, migration, and differentiation of NSC progeny, which fail to migrate through the irradiated RMS and generate neurons in the OB, even following the transplantation of healthy NSCs into the irradiated SEZ.[7,26,30,62,63] Herein, we demonstrate that metformin preTx was able to rescue neuroblast proliferation in both the SEZ and RMS, suggesting that metformin directly enhances neuroblast survival or proliferation or that metformin attenuates IR-induced niche perturbations to maintain a microenvironment that supports neuroblast survival and proliferation. Indeed, the dramatic inhibition of microglia proliferation along the RMS supports the hypothesis that metformin's anti-inflammatory properties may regulate neural precursor behavior. Interestingly, metformin is known to inhibit NF-κB, and the absence of NF-κB-dependent expression of C-C chemokine receptor 2 (CCR2) or its ligand CCL2 is sufficient to reduce chronic microglial activation and rescue both hippocampal neurogenesis and cognitive impairments following cranial IR.[51,64] It is plausible that metformin's inhibitory effects on NF-κB have a priming effect on microglia, reducing their activation capacity and secretion of proinflammatory cytokines or reactive oxygen species in the presence of an injury, such as cranial IR. Therefore, further investigation into metformin's direct effects on microglia are warranted.

It is well recognized that the neurogenic niche plays a fundamental role in regulating NSC behavior and neurogenesis,[16,18] and our findings reveal that factors in the irradiated niche were sufficient to reduce *in vitro* neurosphere formation. Although the specific factors in the conditioned media from the irradiated SEZ were not identified in this study, others have identified factors secreted by vascular endothelial cells and microglia following IR that promote apoptosis and reduced neurogenesis, such as transforming growth factor-β (TGF-β) and interleukin-6 (IL-6), respectively.[28,63,65] Importantly, metformin preTx has been shown to reduce *in vivo* microgliosis, NF-κB activity, and levels of tumor necrosis factor alpha (TNF-α), IL-6, and IL-1β in a rodent stroke model,[43] as well as *in vitro* microglial secretion of TNF-α and IL-6 in the presence of lipopolysaccharide or S100 calcium-binding protein A8.[66,67] Thus, understanding the specific factor(s) that regulate NSC behavior has important implications for neuro-regenerative strategies.

Finally, this study demonstrates that metformin preTx promotes functional recovery in a clinically relevant model of juvenile cranial IR.[8] Accordingly, improved function was correlated with a metformin preTx-induced rescue of neuroblast proliferation in the SEZ and RMS, an increase in neuroblast arrival in the OB, and rescue of newborn neurons in the OB. Although there is controversy around the extent of neurogenesis in adult humans, with studies suggesting that human neurogenesis declines after early childhood,[68–70] recent findings support the theory that neurogenesis persists late into adulthood, at least in the hippocampus.[71,72] In rodents, it is well recognized that the primary function of NSCs in the SEZ is OB neurogenesis, likely playing a necessary role in important behaviors related to reproductive success, such as mate selection and recognition, as well as paternal recognition of offspring.[73–75]

The implications of SEZ-derived neurogenesis on olfactory discrimination remains controversial, and careful consideration of the impact of the neurogenic manipulations may provide insight into the disparate study outcomes. Our use of whole-brain cranial IR affects not only neurogenesis in the SEZ but also other brain regions implicated in olfactory information processing. Importantly, Kouremenou et al.[76] provided a comprehensive summary of studies that have examined the role of neurogenesis in olfactory discrimination tasks and highlighted the conclusion that impairing adult neurogenesis generally diminishes fine odor discrimination. Although several studies suggest that neurogenesis is required for long-term olfactory memory, there is no consensus, which may be attributed to differences in neurogenic manipulations, ranging from more-specific genetic ablation strategies to broader approaches, such as antimitotic treatment and cranial IR.[32,76,77] Overall, the paucity of studies done in juvenile models of injury is notable and worthy of further investigation, as neuroplasticity is well documented to be modified through aging.[78]

Various brain injuries, including stroke, also elicit a neurogenic response from the SEZ, suggesting that SEZ NSCs play an important role not only in OB neurogenesis but in neurorepair.[17,35,79,80] Thus, this study provides strong rationale for further investigation of metformin's potential to stimulate or enhance neurorepair both in other injury models and in clinical trials. Important next steps include assessing metformin's effects in models of primary brain tumors and fractionated doses of cranial IR, as well as in combination with other anti-inflammatory drugs.

Limitations of study

A limitation of this study includes the use of whole-brain, single-dose cranial IR rather than fractionated doses with a focal boost. Future studies investigating the effects of different IR dose schedules are warranted to improve translational outcomes. Similarly, whole-brain irradiation rather than targeted ablation of SEZ-OB neurogenesis precluded our ability to distinguish the direct effects of cranial IR versus indirect effects of inflammation and secondary damage to surrounding tissue, when assessing olfactory memory.

This study investigated the effects of neonatal metformin administration, which has reported age-dependent effects on NSCs.[36] However, given our findings revealing that metformin mitigates cranial-IR-induced deficits by attenuating the inflammatory response and/or enhancing neuroblast migration to the OB, rather than by expanding the NSC pool, future efforts should investigate metformin's effects in the brain throughout aging and as a post-treatment strategy.

(D) Representative images of the anterior RMS 30 days post-IR (solid arrow, Iba1$^+$Ki67$^+$ cell; empty arrow, Iba1$^+$Ki67$^-$ cell; i, scale bar represents 200 μm; ii, scale bar represents 50 μm; blue, DAPI; green, Ki67; red, Iba1).

(E and F) Fold change in the number of (E) Iba1$^+$Ki67$^+$ and (F) Iba1$^+$CD68$^+$ microglia 30 days post-IR (n = 3–4 mice/group; $^{**}p < 0.01$; $^{***}p < 0.001$; one-way ANOVA with Tukey's test).

Data are presented as mean ± SEM.

STAR★METHODS

Detailed methods are provided in the online version of this paper and include the following:

- KEY RESOURCES TABLE
- RESOURCE AVAILABILITY
  - Lead contact
  - Materials availability
  - Data and code availability
- EXPERIMENTAL MODEL AND SUBJECT DETAILS
  - Animals
- METHOD DETAILS
  - Metformin and EdU administration
  - Cranial irradiation
  - Neurosphere assay
  - Fluorescence-activated cell sorting (FACS)
  - Immunohistochemistry
  - Long-term olfactory memory (LTOM) task
- QUANTIFICATION AND STATISTICAL ANALYSIS

SUPPLEMENTAL INFORMATION

Supplemental information can be found online at https://doi.org/10.1016/j.xcrm.2021.100231.

ACKNOWLEDGMENTS

The authors would like to thank members of the Morshead laboratory for critical feedback, as well as Ashkan Azimi and Drs. Rebecca Rudy, Ricky Siu, and Emily Gilbert for technical expertise. This research was funded by Brain Canada, Ontario Institute for Regenerative Medicine, CFREF - Medicine by Design, and the Stem Cell Network.

AUTHOR CONTRIBUTIONS

Conceptualization, D.D. and C.M.M.; methodology, D.D. and C.M.M.; investigation, D.D., T.K., M.R., M.H., N.L., and C.M.M.; formal analysis, D.D., T.K., and M.R.; writing – original draft, D.D.; writing – review & editing, D.D. and C.M.M.; supervision, C.M.M.; funding acquisition, C.M.M.

DECLARATION OF INTERESTS

The authors declare no competing interests.

INCLUSION AND DIVERSITY

We worked to ensure sex balance in the selection of non-human subjects. One or more of the authors of this paper self-identifies as an underrepresented ethnic minority in science. The author list of this paper includes contributors from the location where the research was conducted who participated in the data collection, design, analysis, and/or interpretation of the work.

Received: May 6, 2020
Revised: September 12, 2020
Accepted: March 9, 2021
Published: April 6, 2021

REFERENCES

1. Mabbott, D.J., Spiegler, B.J., Greenberg, M.L., Rutka, J.T., Hyder, D.J., and Bouffet, E. (2005). Serial evaluation of academic and behavioral outcome after treatment with cranial radiation in childhood. J. Clin. Oncol. *23*, 2256–2263.
2. Redmond, K.J., Mahone, E.M., Terezakis, S., Ishaq, O., Ford, E., McNutt, T., Kleinberg, L., Cohen, K.J., Wharam, M., and Horska, A. (2013). Association between radiation dose to neuronal progenitor cell niches and temporal lobes and performance on neuropsychological testing in children: a prospective study. Neuro-oncol. *15*, 360–369.
3. Brinkman, T.M., Krasin, M.J., Liu, W., Armstrong, G.T., Ojha, R.P., Sadighi, Z.S., Gupta, P., Kimberg, C., Srivastava, D., Merchant, T.E., et al. (2016). Long-term neurocognitive functioning and social attainment in adult survivors of pediatric CNS tumors: results from the St Jude Lifetime Cohort Study. J. Clin. Oncol. *34*, 1358–1367.
4. Ma, T.M., Grimm, J., McIntyre, R., Anderson-Keightly, H., Kleinberg, L.R., Hales, R.K., Moore, J., Vannorsdall, T., and Redmond, K.J. (2017). A prospective evaluation of hippocampal radiation dose volume effects and memory deficits following cranial irradiation. Radiother. Oncol. *125*, 234–240.
5. Spiegler, B.J., Bouffet, E., Greenberg, M.L., Rutka, J.T., and Mabbott, D.J. (2004). Change in neurocognitive functioning after treatment with cranial radiation in childhood. J. Clin. Oncol. *22*, 706–713.
6. Tonning Olsson, I., Perrin, S., Lundgren, J., Hjorth, L., and Johanson, A. (2014). Long-term cognitive sequelae after pediatric brain tumor related to medical risk factors, age, and sex. Pediatr. Neurol. *51*, 515–521.
7. Monje, M.L., Mizumatsu, S., Fike, J.R., and Palmer, T.D. (2002). Irradiation induces neural precursor-cell dysfunction. Nat. Med. *8*, 955–962.
8. Ruddy, R.M., Derkach, D., Dadwal, P., and Morshead, C.M. (2020). Cranial irradiation in juvenile mice leads to early and sustained defects in the stem and progenitor cell pools and late cognitive impairments. Brain Res. *1727*, 146548.
9. Lois, C., and Alvarez-Buylla, A. (1993). Proliferating subventricular zone cells in the adult mammalian forebrain can differentiate into neurons and glia. Proc. Natl. Acad. Sci. USA *90*, 2074–2077.
10. Zhao, C., Deng, W., and Gage, F.H. (2008). Mechanisms and functional implications of adult neurogenesis. Cell *132*, 645–660.
11. Doetsch, F., García-Verdugo, J.M., and Alvarez-Buylla, A. (1997). Cellular composition and three-dimensional organization of the subventricular germinal zone in the adult mammalian brain. J. Neurosci. *17*, 5046–5061.
12. Ming, G.L., and Song, H. (2011). Adult neurogenesis in the mammalian brain: significant answers and significant questions. Neuron *70*, 687–702.
13. Whitman, M.C., and Greer, C.A. (2009). Adult neurogenesis and the olfactory system. Prog. Neurobiol. *89*, 162–175.
14. Zou, J., Pan, Y.-W., Wang, Z., Chang, S.-Y., Wang, W., Wang, X., Tournier, C., Storm, D.R., and Xia, Z. (2012). Targeted deletion of ERK5 MAP kinase in the developing nervous system impairs development of GABAergic interneurons in the main olfactory bulb and behavioral discrimination between structurally similar odorants. J. Neurosci. *32*, 4118–4132.
15. Yamashita, T., Ninomiya, M., Hernández Acosta, P., García-Verdugo, J.M., Sunabori, T., Sakaguchi, M., Adachi, K., Kojima, T., Hirota, Y., Kawase, T., et al. (2006). Subventricular zone-derived neuroblasts migrate and differentiate into mature neurons in the post-stroke adult striatum. J. Neurosci. *26*, 6627–6636.
16. Silva-Vargas, V., Crouch, E.E., and Doetsch, F. (2013). Adult neural stem cells and their niche: a dynamic duo during homeostasis, regeneration, and aging. Curr. Opin. Neurobiol. *23*, 935–942.
17. Faiz, M., Sachewsky, N., Gascón, S., Bang, K.W.A., Morshead, C.M., and Nagy, A. (2015). Adult neural stem cells from the subventricular zone give rise to reactive astrocytes in the cortex after stroke. Cell Stem Cell *17*, 624–634.
18. Ruddy, R.M., and Morshead, C.M. (2018). Home sweet home: the neural stem cell niche throughout development and after injury. Cell Tissue Res. *371*, 125–141.
19. Shinohara, C., Gobbel, G.T., Lamborn, K.R., Tada, E., and Fike, J.R. (1997). Apoptosis in the subependyma of young adult rats after single and fractionated doses of X-rays. Cancer Res. *57*, 2694–2702.

20. Chow, B.M., Li, Y.-Q., and Wong, C.S. (2000). Radiation-induced apoptosis in the adult central nervous system is p53-dependent. Cell Death Differ. *7*, 712–720.

21. Bellinzona, M., Gobbel, G.T., Shinohara, C., and Fike, J.R. (1996). Apoptosis is induced in the subependyma of young adult rats by ionizing irradiation. Neurosci. Lett. *208*, 163–166.

22. Acharya, M.M., Lan, M.L., Kan, V.H., Patel, N.H., Giedzinski, E., Tseng, B.P., and Limoli, C.L. (2010). Consequences of ionizing radiation-induced damage in human neural stem cells. Free Radic. Biol. Med. *49*, 1846–1855.

23. Molofsky, A.V., Slutsky, S.G., Joseph, N.M., He, S., Pardal, R., Krishnamurthy, J., Sharpless, N.E., and Morrison, S.J. (2006). Increasing p16INK4a expression decreases forebrain progenitors and neurogenesis during ageing. Nature *443*, 448–452.

24. Zou, Y., Zhang, N., Ellerby, L.M., Davalos, A.R., Zeng, X., Campisi, J., and Desprez, P.-Y. (2012). Responses of human embryonic stem cells and their differentiated progeny to ionizing radiation. Biochem. Biophys. Res. Commun. *426*, 100–105.

25. Cheng, Z., Zheng, Y.Z., Li, Y.-Q., and Wong, C.S. (2017). Cellular senescence in mouse hippocampus after irradiation and the role of p53 and p21. J. Neuropathol. Exp. Neurol. *76*, 260–269.

26. Fukuda, A., Fukuda, H., Swanpalmer, J., Hertzman, S., Lannering, B., Marky, I., Björk-Eriksson, T., and Blomgren, K. (2005). Age-dependent sensitivity of the developing brain to irradiation is correlated with the number and vulnerability of progenitor cells. J. Neurochem. *92*, 569–584.

27. Han, W., Umekawa, T., Zhou, K., Zhang, X.-M., Ohshima, M., Dominguez, C.A., Harris, R.A., Zhu, C., and Blomgren, K. (2016). Cranial irradiation induces transient microglia accumulation, followed by long-lasting inflammation and loss of microglia. Oncotarget *7*, 82305–82323.

28. Monje, M.L., Toda, H., and Palmer, T.D. (2003). Inflammatory blockade restores adult hippocampal neurogenesis. Science *302*, 1760–1765.

29. Wong, C.S., and Van der Kogel, A.J. (2004). Mechanisms of radiation injury to the central nervous system: implications for neuroprotection. Mol. Interv. *4*, 273–284.

30. Hellström, N.A.K., Björk-Eriksson, T., Blomgren, K., and Kuhn, H.G. (2009). Differential recovery of neural stem cells in the subventricular zone and dentate gyrus after ionizing radiation. Stem Cells *27*, 634–641.

31. Ayoub, R., Ruddy, R.M., Cox, E., Oyefiade, A., Derkach, D., Laughlin, S., Ades-Aron, B., Shirzadi, Z., Fieremans, E., MacIntosh, B.J., et al. (2020). Assessment of cognitive and neural recovery in survivors of pediatric brain tumors in a pilot clinical trial using metformin. Nat. Med. *26*, 1285–1294.

32. Lazarini, F., Mouthon, M.-A., Gheusi, G., de Chaumont, F., Olivo-Marin, J.-C., Lamarque, S., Abrous, D.N., Boussin, F.D., and Lledo, P.-M. (2009). Cellular and behavioral effects of cranial irradiation of the subventricular zone in adult mice. PLoS ONE *4*, e7017.

33. Miller, F.D., and Kaplan, D.R. (2012). Mobilizing endogenous stem cells for repair and regeneration: are we there yet? Cell Stem Cell *10*, 650–652.

34. Wang, J., Gallagher, D., DeVito, L.M., Cancino, G.I., Tsui, D., He, L., Keller, G.M., Frankland, P.W., Kaplan, D.R., and Miller, F.D. (2012). Metformin activates an atypical PKC-CBP pathway to promote neurogenesis and enhance spatial memory formation. Cell Stem Cell *11*, 23–35.

35. Dadwal, P., Mahmud, N., Sinai, L., Azimi, A., Fatt, M., Wondisford, F.E., Miller, F.D., and Morshead, C.M. (2015). Activating endogenous neural precursor cells using metformin leads to neural repair and functional recovery in a model of childhood brain injury. Stem Cell Reports *5*, 166–173.

36. Ruddy, R.M., Adams, K.V., and Morshead, C.M. (2019). Age- and sex-dependent effects of metformin on neural precursor cells and cognitive recovery in a model of neonatal stroke. Sci. Adv. *5*, eaax1912.

37. Zhou, G., Myers, R., Li, Y., Chen, Y., Shen, X., Fenyk-Melody, J., Wu, M., Ventre, J., Doebber, T., Fujii, N., et al. (2001). Role of AMP-activated protein kinase in mechanism of metformin action. J. Clin. Invest. *108*, 1167–1174.

38. Martin-Montalvo, A., Mercken, E.M., Mitchell, S.J., Palacios, H.H., Mote, P.L., Scheibye-Knudsen, M., Gomes, A.P., Ward, T.M., Minor, R.K., Blouin, M.-J., et al. (2013). Metformin improves healthspan and lifespan in mice. Nat. Commun. *4*, 2192.

39. Jin, Q., Cheng, J., Liu, Y., Wu, J., Wang, X., Wei, S., Zhou, X., Qin, Z., Jia, J., and Zhen, X. (2014). Improvement of functional recovery by chronic metformin treatment is associated with enhanced alternative activation of microglia/macrophages and increased angiogenesis and neurogenesis following experimental stroke. Brain Behav. Immun. *40*, 131–142.

40. Liu, Y., Tang, G., Zhang, Z., Wang, Y., and Yang, G.-Y. (2014). Metformin promotes focal angiogenesis and neurogenesis in mice following middle cerebral artery occlusion. Neurosci. Lett. *579*, 46–51.

41. Yuan, R., Wang, Y., Li, Q., Zhen, F., Li, X., Lai, Q., Hu, P., Wang, X., Zhu, Y., Fan, H., and Yao, R. (2019). Metformin reduces neuronal damage and promotes neuroblast proliferation and differentiation in a cerebral ischemia/reperfusion rat model. Neuroreport *30*, 232–240.

42. Saisho, Y. (2015). Metformin and inflammation: its potential beyond glucose-lowering effect. Endocr. Metab. Immune Disord. Drug Targets *15*, 196–205.

43. Zhu, X.-C., Jiang, T., Zhang, Q.-Q., Cao, L., Tan, M.-S., Wang, H.-F., Ding, Z.-Z., Tan, L., and Yu, J.-T. (2015). Chronic metformin preconditioning provides neuroprotection via suppression of NF-κB-mediated inflammatory pathway in rats with permanent cerebral ischemia. Mol. Neurobiol. *52*, 375–385.

44. Wang, C., Liu, C., Gao, K., Zhao, H., Zhou, Z., Shen, Z., Guo, Y., Li, Z., Yao, T., and Mei, X. (2016). Metformin preconditioning provide neuroprotection through enhancement of autophagy and suppression of inflammation and apoptosis after spinal cord injury. Biochem. Biophys. Res. Commun. *477*, 534–540.

45. Sato, Y., Shinjyo, N., Sato, M., Nilsson, M.K.L., Osato, K., Zhu, C., Pekna, M., Kuhn, H.G., and Blomgren, K. (2018). Grafting neural stem and progenitor cells into the hippocampus of juvenile, irradiated mice normalizes behavior deficits. Front. Neurol. *9*, 715.

46. Dutta, S., and Sengupta, P. (2016). Men and mice: relating their ages. Life Sci. *152*, 244–248.

47. Codega, P., Silva-Vargas, V., Paul, A., Maldonado-Soto, A.R., Deleo, A.M., Pastrana, E., and Doetsch, F. (2014). Prospective identification and purification of quiescent adult neural stem cells from their in vivo niche. Neuron *82*, 545–559.

48. Jiang, T., Yu, J.-T., Zhu, X.-C., Wang, H.-F., Tan, M.-S., Cao, L., Zhang, Q.-Q., Gao, L., Shi, J.-Q., Zhang, Y.-D., and Tan, L. (2014). Acute metformin preconditioning confers neuroprotection against focal cerebral ischaemia by pre-activation of AMPK-dependent autophagy. Br. J. Pharmacol. *171*, 3146–3157.

49. Zhuo, L., Sun, B., Zhang, C.L., Fine, A., Chiu, S.Y., and Messing, A. (1997). Live astrocytes visualized by green fluorescent protein in transgenic mice. Dev. Biol. *187*, 36–42.

50. Zou, J., Wang, W., Pan, Y.-W., Lu, S., and Xia, Z. (2015). Methods to measure olfactory behavior in mice. Curr. Protoc. Toxicol. *63*, 11.18.1–11.18.21.

51. Lee, S.W., Haditsch, U., Cord, B.J., Guzman, R., Kim, S.J., Boettcher, C., Priller, J., Ormerod, B.K., and Palmer, T.D. (2013). Absence of CCL2 is sufficient to restore hippocampal neurogenesis following cranial irradiation. Brain Behav. Immun. *30*, 33–44.

52. Daynac, M., Chicheportiche, A., Pineda, J.R., Gauthier, L.R., Boussin, F.D., and Mouthon, M.-A. (2013). Quiescent neural stem cells exit dormancy upon alteration of GABAAR signaling following radiation damage. Stem Cell Res. (Amst.) *11*, 516–528.

53. Fatt, M., Hsu, K., He, L., Wondisford, F., Miller, F.D., Kaplan, D.R., and Wang, J. (2015). Metformin acts on two different molecular pathways to enhance adult neural precursor proliferation/self-renewal and differentiation. Stem Cell Reports *5*, 988–995.

54. Obernier, K., Cebrian-Silla, A., Thomson, M., Parraguez, J.I., Anderson, R., Guinto, C., Rodas Rodriguez, J., Garcia-Verdugo, J.-M., and Alvarez-Buylla,

A. (2018). Adult neurogenesis is sustained by symmetric self-renewal and differentiation. Cell Stem Cell *22*, 221–234.e8.

55. Imayoshi, I., Sakamoto, M., Yamaguchi, M., Mori, K., and Kageyama, R. (2010). Essential roles of Notch signaling in maintenance of neural stem cells in developing and adult brains. J. Neurosci. *30*, 3489–3498.
56. Kawaguchi, D., Furutachi, S., Kawai, H., Hozumi, K., and Gotoh, Y. (2013). Dll1 maintains quiescence of adult neural stem cells and segregates asymmetrically during mitosis. Nat. Commun. *4*, 1880.
57. Liu, X., Wang, Q., Haydar, T.F., and Bordey, A. (2005). Nonsynaptic GABA signaling in postnatal subventricular zone controls proliferation of GFAP-expressing progenitors. Nat. Neurosci. *8*, 1179–1187.
58. Kokovay, E., Wang, Y., Kusek, G., Wurster, R., Lederman, P., Lowry, N., Shen, Q., and Temple, S. (2012). VCAM1 is essential to maintain the structure of the SVZ niche and acts as an environmental sensor to regulate SVZ lineage progression. Cell Stem Cell *11*, 220–230.
59. Ottone, C., Krusche, B., Whitby, A., Clements, M., Quadrato, G., Pitulescu, M.E., Adams, R.H., and Parrinello, S. (2014). Direct cell-cell contact with the vascular niche maintains quiescent neural stem cells. Nat. Cell Biol. *16*, 1045–1056.
60. Porlan, E., Martí-Prado, B., Morante-Redolat, J.M., Consiglio, A., Delgado, A.C., Kypta, R., López-Otín, C., Kirstein, M., and Fariñas, I. (2014). MT5-MMP regulates adult neural stem cell functional quiescence through the cleavage of N-cadherin. Nat. Cell Biol. *16*, 629–638.
61. Morizur, L., Chicheportiche, A., Gauthier, L.R., Daynac, M., Boussin, F.D., and Mouthon, M.-A. (2018). Distinct molecular signatures of quiescent and activated adult neural stem cells reveal specific interactions with their microenvironment. Stem Cell Reports *11*, 565–577.
62. Achanta, P., Capilla-Gonzalez, V., Purger, D., Reyes, J., Sailor, K., Song, H., Garcia-Verdugo, J.M., Gonzalez-Perez, O., Ford, E., and Quinones-Hinojosa, A. (2012). Subventricular zone localized irradiation affects the generation of proliferating neural precursor cells and the migration of neuroblasts. Stem Cells *30*, 2548–2560.
63. Pineda, J.R., Daynac, M., Chicheportiche, A., Cebrian-Silla, A., Sii Felice, K., Garcia-Verdugo, J.M., Boussin, F.D., and Mouthon, M.-A. (2013). Vascular-derived TGF-β increases in the stem cell niche and perturbs neurogenesis during aging and following irradiation in the adult mouse brain. EMBO Mol. Med. *5*, 548–562.
64. Belarbi, K., Jopson, T., Arellano, C., Fike, J.R., and Rosi, S. (2013). CCR2 deficiency prevents neuronal dysfunction and cognitive impairments induced by cranial irradiation. Cancer Res. *73*, 1201–1210.
65. Patel, R.K., Prasad, N., Kuwar, R., Haldar, D., and Abdul-Muneer, P.M. (2017). Transforming growth factor-beta 1 signaling regulates neuroinflammation and apoptosis in mild traumatic brain injury. Brain Behav. Immun. *64*, 244–258.
66. Ha, J.-S., Yeom, Y.-S., Jang, J.-H., Kim, Y.-H., Im, J.I., Kim, I.S., and Yang, S.-J. (2019). Anti-inflammatory effects of metformin on neuro-inflammation and NLRP3 inflammasome activation in BV-2 microglial cells. Biomed. Sci. Lett. *25*, 92–98.
67. Wang, H., Guo, Y., Yao, H., Li, M., Yuan, Z., Zhang, J., Jiang, W., and Li, Y. (2019). Metformin inhibits LPS-stimulated microglial proliferation and reduces the release of inflammatory cytokines. Int. J. Clin. Exp. Med. *12*, 2201–2208.
68. Dennis, C.V., Suh, L.S., Rodriguez, M.L., Kril, J.J., and Sutherland, G.T. (2016). Human adult neurogenesis across the ages: an immunohistochemical study. Neuropathol. Appl. Neurobiol. *42*, 621–638.
69. Andreae, L.C. (2018). Adult neurogenesis in humans: dogma overturned, again and again? Sci. Transl. Med. *10*, eaat3893.
70. Sorrells, S.F., Paredes, M.F., Cebrian-Silla, A., Sandoval, K., Qi, D., Kelley, K.W., James, D., Mayer, S., Chang, J., Auguste, K.I., et al. (2018). Human hippocampal neurogenesis drops sharply in children to undetectable levels in adults. Nature *555*, 377–381.
71. Boldrini, M., Fulmore, C.A., Tartt, A.N., Simeon, L.R., Pavlova, I., Poposka, V., Rosoklija, G.B., Stankov, A., Arango, V., Dwork, A.J., et al. (2018). Human hippocampal neurogenesis persists throughout aging. Cell Stem Cell *22*, 589–599.e5.
72. Moreno-Jiménez, E.P., Flor-García, M., Terreros-Roncal, J., Rábano, A., Cafini, F., Pallas-Bazarra, N., Ávila, J., and Llorens-Martín, M. (2019). Adult hippocampal neurogenesis is abundant in neurologically healthy subjects and drops sharply in patients with Alzheimer's disease. Nat. Med. *25*, 554–560.
73. Mak, G.K., Enwere, E.K., Gregg, C., Pakarainen, T., Poutanen, M., Huhtaniemi, I., and Weiss, S. (2007). Male pheromone-stimulated neurogenesis in the adult female brain: possible role in mating behavior. Nat. Neurosci. *10*, 1003–1011.
74. Mak, G.K., and Weiss, S. (2010). Paternal recognition of adult offspring mediated by newly generated CNS neurons. Nat. Neurosci. *13*, 753–758.
75. Oboti, L., Schellino, R., Giachino, C., Chamero, P., Pyrski, M., Leinders-Zufall, T., Zufall, F., Fasolo, A., and Peretto, P. (2011). Newborn interneurons in the accessory olfactory bulb promote mate recognition in female mice. Front. Neurosci. *5*, 113.
76. Kouremenou, I., Piper, M., and Zalucki, O. (2020). Adult neurogenesis in the olfactory system: improving performance for difficult discrimination tasks? BioEssays *42*, e2000065.
77. Sultan, S., Mandairon, N., Kermen, F., Garcia, S., Sacquet, J., and Didier, A. (2010). Learning-dependent neurogenesis in the olfactory bulb determines long-term olfactory memory. FASEB J. *24*, 2355–2363.
78. Lemasson, M., Saghatelyan, A., Olivo-Marin, J.-C., and Lledo, P.-M. (2005). Neonatal and adult neurogenesis provide two distinct populations of newborn neurons to the mouse olfactory bulb. J. Neurosci. *25*, 6816–6825.
79. Zhang, R., Zhang, Z., Wang, L., Wang, Y., Gousev, A., Zhang, L., Ho, K.-L., Morshead, C., and Chopp, M. (2004). Activated neural stem cells contribute to stroke-induced neurogenesis and neuroblast migration toward the infarct boundary in adult rats. J. Cereb. Blood Flow Metab. *24*, 441–448.
80. Thored, P., Arvidsson, A., Cacci, E., Ahlenius, H., Kallur, T., Darsalia, V., Ekdahl, C.T., Kokaia, Z., and Lindvall, O. (2006). Persistent production of neurons from adult brain stem cells during recovery after stroke. Stem Cells *24*, 739–747.
81. Schindelin, J., Arganda-Carreras, I., Frise, E., Kaynig, V., Longair, M., Pietzsch, T., Preibisch, S., Rueden, C., Saalfeld, S., Schmid, B., et al. (2012). Fiji: an open-source platform for biological-image analysis. Nat. Methods *9*, 676–682.
82. Quaile, M.P., Melich, D.H., Jordan, H.L., Nold, J.B., Chism, J.P., Polli, J.W., Smith, G.A., and Rhodes, M.C. (2010). Toxicity and toxicokinetics of metformin in rats. Toxicol. Appl. Pharmacol. *243*, 340–347.
83. Morshead, C.M., Benveniste, P., Iscove, N.N., and van der Kooy, D. (2002). Hematopoietic competence is a rare property of neural stem cells that may depend on genetic and epigenetic alterations. Nat. Med. *8*, 268–273.
84. Coles-Takabe, B.L.K., Brain, I., Purpura, K.A., Karpowicz, P., Zandstra, P.W., Morshead, C.M., and van der Kooy, D. (2008). Don't look: growing clonal versus nonclonal neural stem cell colonies. Stem Cells *26*, 2938–2944.

STAR★METHODS

KEY RESOURCES TABLE

REAGENT or RESOURCE	SOURCE	IDENTIFIER
Antibodies		
Rat monoclonal anti-CD133 (13A4), Biotinylated	Thermo Fisher	Cat# 13-1331-82; RRID: AB_466591
Streptavidin PE-Cyanine7 Conjugate	Thermo Fisher	Cat# 25-4317-82; RRID: AB_10116480
Mouse monoclonal anti-Doublecortin (E-6)	Santa Cruz Biotechnology	Cat# sc-271390; RRID: AB_10610966
Rabbit polyclonal anti-NeuN	Sigma-Aldrich	Cat# ABN78; RRID: AB_10807945
Rabbit polyclonal anti-Ki67	Abcam	Cat# ab15580; RRID: AB_443209
Goat polyclonal anti-AIF-1/Iba1	Novus Biologicals	Cat# NB100-1028; RRID: AB_521594
Rabbit polyclonal anti-Iba1	Wako Chemicals	Cat# 019-19741; RRID: AB_839504
Rat monoclonal anti-mouse CD68 (FA-11)	Bio-Rad	Cat# MCA1957; RRID: AB_322219
Donkey anti-mouse Alexa 568	Thermo Fisher	Cat# A10037; RRID: AB_2534013
Goat anti-rabbit Alexa 488	Thermo Fisher	Cat# A11034; RRID: AB_2576217
Donkey anti-rabbit Alexa 488	Thermo Fisher	Cat# A21206; RRID: AB_2535792
Donkey anti-goat Alexa 568	Thermo Fisher	Cat# A11057; RRID: AB_2534104
Donkey anti-rat Alexa 594	Thermo Fisher	Cat# A21209; RRID: AB_2535795
Chemicals, peptides, and recombinant proteins		
2,2,2-tribromoethanol	Sigma-Aldrich	Cat# T48402
Metformin (1,1-dimethylbiguanide hydrochloride)	Sigma-Aldrich	Cat# D150959
DAPI	Thermo Fisher	Cat# D1306; RRID: AB_2629482
EdU (5-ethynyl-2′-deoxyuridine)	Thermo Fisher	Cat# E10187
EGF-Alexa 647 Conjugate	Thermo Fisher	Cat# E35351
Isoamyl acetate	Sigma-Aldrich	Cat# W205508
Citralva (3,7-dimethyl-2,6-octadienenitrile)	Sigma-Aldrich	Cat# W512508
Critical commercial assays		
Click-iT EdU Alexa 647 Flow Cytometry Assay Kit	Thermo Fisher	Cat# C10424
Experimental models: Organisms/strains		
C57BL/6	Charles River Laboratories	RRID: IMSR_CRL:27
FVB/N-Tg(GFAPGFP)14Mes/J	The Jackson Laboratory	RRID: IMSR_JAX:003257
Software and algorithms		
BD FACSDiva	BD Biosciences	https://www.bdbiosciences.com/en-us/instruments/research-instruments/research-software/flow-cytometry-acquisition/facsdiva-software
FlowJo 9.3	FlowJo LLC	https://www.flowjo.com/
Zen	Zeiss	https://www.zeiss.com/microscopy/int/products/microscope-software/zen.html
Fiji	Schindelin et al.[81]	https://imagej.net/Fiji
Prism 6	GraphPad Software	https://www.graphpad.com/scientific-software/prism/
Other		
20mg sucrose pellets	Bio-Serv	Cat# F05550

RESOURCE AVAILABILITY

Lead contact

Further information and requests for resources and reagents should be directed to and will be fulfilled by the lead contact, Dr. Cindi Morshead (cindi.morshead@utoronto.ca).

Materials availability

This study did not generate new unique reagents or materials.

Data and code availability

The published article includes all data generated or analyzed during this study. There was no new code developed as part of this study.

EXPERIMENTAL MODEL AND SUBJECT DETAILS

Animals

Young adult (6-week-old) C57BL/6 mice were purchased from Charles River (Montreal, Canada) for breeding. For FACS experiments, transgenic hGFAP::GFP mice expressing green fluorescent protein (GFP) under the control of the human GFAP promoter were purchased from The Jackson Laboratory (#003257; Maine, USA). Male and female mice were used for all experiments and were randomly allocated to experimental groups. All mice were group-housed and maintained on a 12-hour day/night light cycle. Food and water were available *ad libitum*, except for mice undergoing the LTOM task, in which food was restricted as described below. Mice were euthanized via anesthetic overdose using an intraperitoneal (IP) injection of avertin (2,2,2-tribromoethanol, Sigma-Aldrich), followed by cervical dislocation and decapitation for neurosphere assay and FACS experiments, or transcardial perfusion with 4% paraformaldehyde (PFA). All animal work was performed in accordance with institutional guidelines and approved by the University of Toronto Animal Care Committee.

METHOD DETAILS

Metformin and EdU administration

Metformin (1,1-dimethylbiguanide hydrochloride, Sigma-Aldrich, D150959) was dissolved in sterile PBS (20mg/mL) and administered once daily via subcutaneous injection at 200mg/kg body weight,[36] a dose that has been reported to be safe for long-term rodent administration.[82] PBS was administered as a vehicle control. EdU (50mg/kg, Thermo Fisher, E10187) was administered via single daily IP injections for 4 days starting on the final day of LTOM acquisition (P54-57).

Cranial irradiation

Cranial irradiation was performed as previously described.[8] Briefly, mice were anaesthetized on P17 via IP injection of avertin (250mg/kg body weight 2,2,2-tribromoethanol), secured inside a lead shield exposing only the head, and placed in a cesium-137 gamma irradiator (Best Theratronics, Gamacell 40 Exactor). Mice received 8 grays (Gy) of whole brain cranial IR at a rate of ~1 Gy/minute. Following cranial IR, mice were returned to their home cage where they recovered under a heat lamp.

Neurosphere assay

Mice were sacrificed as described and brains were removed and placed in ice cold artificial cerebrospinal fluid (aCSF). The SEZ of both hemispheres was dissected as previously described.[35,83] Tissue was treated with an enzyme solution consisting of 1.33mg/mL trypsin (Sigma-Aldrich, T1005), 1245 units/mL (~0.76mg/mL) hyaluronidase (Sigma-Aldrich, H6254), and 0.13mg/mL kynurenic acid (Sigma-Aldrich, K3375) in aCSF. During enzymatic digestion, samples were incubated on a rocker at 37°C for 25 minutes and then centrifuged for 5 minutes at 1500rpm. The supernatant was removed and replaced with a trypsin inhibitor solution consisting of 0.67mg/mL ovomucoid (Worthington, LS003086) in serum-free media (SFM). Samples were triturated 30x with a P1000 micropipette to dissociate tissue into single cells and centrifuged for 5 minutes at 1500rpm. Cells were resuspended in SFM supplemented with mitogens (20ng/mL epidermal growth factor (EGF; GIBCO, PMG8041), 10ng/mL basic fibroblast growth factor (bFGF; GIBCO, PHG0266), and 2 μg/mL heparin (Sigma-Aldrich, H3149); EFH) and triturated 10x with a P1000 micropipette. Samples were centrifuged, resuspended in SFM+EFH, plated at 10 cells/μL[84] in SFM+EFH, and incubated at 37°C with 5% CO_2. Neurospheres were counted after 7 days of undisturbed incubation.

For conditioned media experiments, mice were euthanized on P18, and brains were isolated and dissected as described. The SEZ tissue from 3 brains per group (Control, IR, and IR+Met) was pooled, digested, and suspended in SFM+EFH at 40 cells/μL for 24 hours. Samples were collected, centrifuged for 5 minutes at 1500rpm, and supernatant was collected and filtered for use as conditioned media. Conditioned media was not re-supplemented with mitogens. SEZ tissue was isolated from P19 non-irradiated control mice and processed as described. Cells were plated in SFM+EFH alone, control conditioned media (from non-irradiated mice), IR conditioned media (from cranially irradiated mice), or IR+Met conditioned media (from cranially irradiated, metformin pre-treated mice) at 10 cells/μL and incubated at 37°C for 7 days before neurospheres were counted.

Fluorescence-activated cell sorting (FACS)

GFAP::GFP mice were sacrificed on P19 and the SEZ tissue from 5 mice per treatment group was pooled in order to obtain a sufficient number of SEZ cells per FACS run as previously described.[47] Wild-type mice were used for generating single color and fluorescence minus one (FMO) controls. Tissue was dissociated with papain (Worthington, LS003127) for 10 minutes at 37°C and

centrifuged for 5 minutes at 1300rpm at 4°C. The supernatant was replaced with DMEM/F12 (DMEM from GIBCO, 12100046; F12 from GIBCO, 21700075), which was supplemented with ovomucoid solution (7mg/mL; Worthington, LS003086) and DNase (15mg/mL; Worthington, LK003172). Samples were triturated 50x with a P200 micropipette and centrifuged through a 22% Percoll (Sigma-Aldrich, P4937) gradient for 10 minutes at 1800rpm at 4°C. Upon removing myelin residuals and Percoll, samples were resuspended in staining solution and centrifuged for 5 minutes at 1300rpm at 4°C.

5 single color controls (unstained, DAPI, PE-Cy7, A647, GFP) and 3 FMO controls (GFAP::GFP, CD133-PE-Cy7, EGF-A647) were prepared for adjusting compensation parameters and setting gates, respectively. CD133 (prominin-1) was labeled using an anti-CD133-biotin antibody (Thermo Fisher, 13-1331-82) at a concentration of 1:300 in staining solution. Samples were incubated on ice for 15 minutes, washed with staining solution, and centrifuged for 5 minutes at 1300rpm at 4°C. The supernatant was replaced with staining solution, and Streptavidin-PE-Cy7 (Thermo Fisher, 25-4317-82) at 1:1000 was added to bind anti-CD133-biotin, while EGFR was labeled by EGF conjugated to Alexa Fluor 647 (EGF-A647; Thermo Fisher, E35351) at 1:300. Upon adding streptavidin-PE-Cy7 and EGF-A647, samples were incubated on ice for 15 minutes, washed with staining solution, and centrifuged for 5 minutes at 1300rpm at 4°C prior to resuspension in staining solution. DAPI (Thermo Fisher, D1306) was added at 1:10,000 and samples were strained through 40 μm nylon cell strainers (Fisher Scientific, 22-363-547).

FACS was conducted using a BD FACS Aria IIIu (BD Biosciences, California, USA) with a sheath pressure of 13psi and 100 μm nozzle aperture. FMO controls were used to set gates and single color controls were used to adjust compensation parameters. BD FACSDiva software (BD Biosciences, California, USA) was used for equipment setup and data acquisition, while FlowJo 9.3 (FlowJo LLC, Oregon, USA) was used for data analysis. Cells were first gated to exclude debris and doublets, followed by DAPI exclusion to gate for live cells. FMO controls were then used to set gates for GFAP::GFP$^+$, CD133$^+$, and EGFR$^+$ populations, allowing isolation of GFAP::GFP$^+$CD133$^+$EGFR$^-$ qNSCs and GFAP::GFP$^+$CD133$^+$EGFR$^+$ aNSCs, and data was presented using biexponential scaling.

Immunohistochemistry

Mice were sacrificed as described and transcardially perfused with ice cold 4% PFA on P19, P47, or P84. Brains were removed and post-fixed in 4% PFA at 4°C for 4-5 hours and cryoprotected in 30% sucrose solution at 4°C until sectioned (20 μm thick) on an HM525 NX Cryostat (Thermo Scientific, 956640). Coronal sections were rehydrated in PBS prior to antigen retrieval (95°C for 15 minutes) in citrate buffer (pH 6.0). Slides were incubated in a blocking solution comprised of 5% normal donkey serum (Sigma-Aldrich, D9663), 10mg/mL bovine serum albumin (Sigma-Aldrich, A9647), and 0.3% Triton X-100 (Sigma-Aldrich, T9284) for 1 hour at room temperature. Primary antibodies were prepared in the same blocking solution and applied to slides for overnight (16 hours) incubation at 4°C. Neuroblasts were labeled using mouse anti-DCX (1:400; Santa Cruz Biotechnology, sc-271390), neurons were labeled using rabbit anti-NeuN (1:250; Sigma-Aldrich, ABN78), proliferating cells were labeled using rabbit anti-Ki67 (1:500; Abcam, ab15580), and microglia were labeled using goat anti-Iba1 (1:200; Novus Biologicals, NB100-1028) for Iba1$^+$Ki67$^+$ labeling (Figure 5E), or rabbit anti-Iba1 (1:500; Wako Chemicals, 019-19741) and rat anti-CD68 (1:500; Bio-Rad, MCA1957) for Iba1$^+$CD68$^+$ labeling (Figure 5F) . The next day, slides were incubated in secondary antibodies (1:750) and 1:10,000 DAPI (Thermo Fisher, D1306) for 90 minutes at room temperature prior to applying mounting medium (Dako, S302380-2) and coverslips. DCX was labeled using donkey anti-mouse Alexa Fluor 568 (Thermo Fisher, A10037), NeuN was labeled using goat anti-rabbit Alexa Fluor 488 (Thermo Fisher, A11034), and Ki67 was labeled using donkey anti-rabbit Alexa Fluor 488 (Thermo Fisher, A21206). For Iba1$^+$Ki67$^+$ labeling, Iba1 was labeled using donkey anti-goat Alexa Fluor 568 (Thermo Fisher, A11057). For Iba1$^+$CD68$^+$ labeling, Iba1 was labeled using goat anti-rabbit Alexa Fluor 488 (Thermo Fisher, A11034) and CD68 was labeled using donkey anti-rat Alexa Fluor 594 (Thermo Fisher, A21209). For EdU staining, slides were additionally incubated in 0.3% Triton X-100 for 20 minutes and a Click-It reaction cocktail containing 1:400 Alexa Fluor 647 azide (Thermo Fisher, C10424) for 30 minutes after antigen retrieval.

Imaging was performed on an Axio Observer Z1 inverted motorized microscope (Zeiss, Germany) with a high-speed spinning disk CSU-X1 confocal scanner unit (Yokogawa, Texas, USA). Zen (Zeiss, Germany) and Fiji[81] software were used for image acquisition and processing. Three sections per animal were quantified based on their rostral-caudal location. For the OB, 3 sections separated by 300μm intervals were counted, with the accessory OB as the posterior limit. For the RMS, 3 sections separated by 300μm intervals were counted, with the frontal pole (rostral tip of cerebral cortex) as the anterior limit. For the SEZ, 3 sections extending from the crossing of the genu of the corpus callosum to the crossing of the anterior commissure were counted. Three regions of interest (ROIs) in the SEZ were analyzed and pooled from each LV. Images of the SEZ (Figure 3B) were tiled upon acquisition using Zen software with 10% overlap between tiles in order to capture the entire lateral ventricle. The dorsolateral corner, the midpoint of the lateral wall, and the ventral corner were analyzed in 150x50 μm ROIs. The total number of DCX$^+$Ki67$^+$ cells in each ROI was counted and expressed as a proportion of DAPI$^+$ cells. All cells were manually counted using the Fiji Cell Counter plugin.

Long-term olfactory memory (LTOM) task

A sand-digging based olfactory discrimination/learning assay was utilized to measure LTOM, in which an odor cue is paired with a food reward.[50] Mice were food restricted prior to and during behavioral training/acquisition (from P37-54) and testing (from P81-84) to maintain 85%–90% of baseline body weight. Prior to acquisition and test sessions, mice were acclimated to a clean, empty cage with bedding for 30 minutes, which was used as the acquisition and testing arena. From P41-43, mice underwent daily acclimation sessions to sugar reward pellets (Bio-Serv, F05550) and the reward/sand delivery apparatus, in which 3 sugar pellets were placed in the

base of a 35x10mm Petri dish atop the reward/sand delivery apparatus. Dishes were filled with autoclaved sand (Canadian Tire, 059-4557-4) for all trials after P41-43 acclimation. From P44-46, mice underwent daily pre-training sessions to learn to dig and retrieve sugar pellets from the sand. The left or right location of the sand-filled dish with a sugar pellet was randomized among the trials.

Following pre-training, mice were trained to associate the reward with isoamyl acetate (IAA; Sigma-Aldrich, W205508), while Citralva (3,7-dimethyl-2,6-octadienenitrile; Sigma-Aldrich, W512508) was used to scent the non-reward dish. Training/acquisition took place for 8 days (P47-54) with 2 blocks of 4 trials per day (1 minute inter-trial interval, 4 hour inter-block interval). On the reward/sand delivery apparatus, both dishes were filled with sand. The dish containing the reward was scented with 100 μL 10mM IAA and the non-reward dish with 100 μL 10mM Citralva. The location of the reward dish containing a buried sugar pellet was randomized between trials. If a mouse dug in the reward dish, the trial was recorded as correct, while digging in the non-reward dish was recorded as incorrect (mice were not permitted to dig in both dishes). Scores were quantified as a percentage of correct trials relative to total acquisition trials on each day.

Mice that correctly chose the reward-associated dish at an average rate of $\geq$ 80% over the final two acquisition days (P53-54) passed the acquisition phase and were tested 1 month after the final acquisition day (P84). Testing on P84 involved a single block of 4 trials (1 minute inter-trial interval) with no reward in either of the scented dishes. As in the acquisition phase, the location of the scented dishes was randomized between trials and mice were only permitted to dig in one dish. Scores were quantified as a percentage of correct trials relative to total testing trials.

QUANTIFICATION AND STATISTICAL ANALYSIS

Experimenters were blinded to groups. All raw data was recorded using Microsoft Excel (Microsoft, Washington, USA). Statistical analyses and graphing were performed using Prism 6 (GraphPad Software, California, USA). All quantified values were presented as group mean ± standard error of the mean (SEM). Column analyses between 2 groups were performed using unpaired t tests, or multiple unpaired t tests when comparing 2 groups over multiple time points. Column analyses between 3 groups were performed using one-way ANOVA with Tukey's test for multiple comparisons. Grouped analysis for LTOM acquisition was performed using two-way ANOVA with Tukey's test for multiple comparisons. A p value < 0.05 was considered statistically significant. The tests used and sample sizes are designated in the figure legends.